
Effect of Aluminum Addition on Microstructure and Oxidation Performance of Cast Irons

Nawal Mohammed Dawood[†], Baraa H. Al khaqani^{†*}, Asia Mishaal Salim[‡]

[†]College of Materials Engineering, University of Babylon, Iraq

[‡]College of Engineering, University of Al- Qadisiyah, Iraq

*Corresponding Author email: mat.baraa.hassan@uobabylon.edu.iq

ABSTRACT: The cast iron that comes with a ferritic matrix are mainly used for the application that require higher temperature working conditions, such as exhaust manifold. However, the higher demand for obtaining material show higher efficiency led the material production companies and manufacturers to use Ni-resist austenitic ductile cast irons and stainless steels, which are relatively more expensive than cast iron and considered as the main challenge for them. This challenge motivated the manufacturer to develop new alloys that show high temperature resistance, higher resistance for oxidation, and lower in cost. In this study, works postulates the resistance of the phases formed due to oxidation of the cast iron alloy with the ratio of (0 to 4 wt% Al) based on the oxidation, X-ray diffraction, and optical microscopy. The oxidation mechanisms of the referred alloy were presented at the range of high temperature (700-900 °C). The results showed the temperature of oxidation and Al content are linearly proportional. Low resistance for the oxidation was noticed at a lower value of oxidation temperature. The oxidation resistance was characterized by the formation of FeO, Fe₂O₃ and Fe₃O₄. The performance of the alloyed cast-irons was significantly enhanced as the content of Al increased. As the content of Al increased, the scale thickness reduced gradually. The behavior of the alloyed cast-irons oxidation kinetic for all conditions of the test was parabolic in its nature at various constants of parabolic rates.

KEYWORDS: high-temperature material, Oxidation Behavior, ductile cast iron, Alloyed Cast Irons.

INTRODUCTION

Hot gases as combustion products delivered from the combustion chamber to the atmosphere [1]. The new designs of the mechanical engine must be designed based on both consumption of fuel and environment satisfactions [2]. The temperature of the exhaust gas might be within order of 1000°C. due to engine operation, a continuous thermal cycles and elevated temperature are fluctuated in its function and that effect the exhaust manifold induced thermal stresses. Furthermore, the several higher temperature oxidation processes occurs due to the flow of the high temperature gas flow. Therefore, resistance to the thermal fatigue, low thermal expansion, and mechanical stability are the critical factor must be taken into the consideration throughout manifold design. The lower values of the thermal expansions and the higher values of the thermal conductivity ensure lower values of the induced thermal stresses at the beginning and the end of the working cycle of the engine [1-5]. Based on what have presented of the thermal stress induced in the manifold, the manufacturers started to find a new material withstand the fluctuation in the temperature and show higher resistance to the thermal stress and oxidation [2-10]. Dissimilar to the ferritic ductile cast irons, the austenitic stainless steels and Ni-resist austenitic ductile cast irons are highly recommended due to its thermal stability [2,5,11].

However, the austenitic alloys are expensive because of the cost manufacturing cost and chemical composition. New material of low unit cost and show good thermal stability and oxidation resistance must be developed [12–13]. In their research, Ekström and Jonsson explained that ferritic alloys showed low thermal expansion and high thermal stability than the austenitic alloys [3]. Though, the A1 temperature of the SiMo alloy is approximately 820°C [4], while the elastic modulus of the SiMo51 decreases as the temperature increases above 700°C [3]. Ti enhance both mechanical and thermal properties at the higher temperature, it is good to develop a ferritic ductile cast iron of higher A1 temperature. In the alloy design of ductile cast iron, high graphite nodularity, high nodule count, and homogeneous graphite distribution can be obtained with hypereutectic composition; thus, C and Si should be selected to obtain a hypereutectic C equivalent (≥ 4.7) for casting and solidification [14]. In order to increase the A1 temperature, in addition to the Si, other elements of alloys, such as Ti, Al, Nb, and W may be

added to the composition [15,16]. Aluminum increases resistance of the oxidation by producing a layer of the stabilized oxide at elevated temperature [6,17]. Mechanical properties can be improved by carbide-forming elements addition, such as Ti, Mo, W, Nb, and Cr up to 1wt% [6,18,19-21]. Among these, Nb and Ti improve the mechanical properties at elevated temperature by producing the primary carbides that are stable at these temperatures [22, 23]. However, their presence is well known to change morphology of the graphite from spheroidal to vermicular, and that result in reducing the mechanical properties. However, the thermal conductivity is enhanced [24-30].

The maximum value of the ferritic SGI temperature (spheroidal graphite cast iron) in service is actually restricted by three phenomena: the phase transition of the ferrite–austenite which change the dimensions, the second phenomena is the decarburization, which increases as the temperatures increase above 800 °C [5]. This phenomenon accompanied with a small variation with Si-content, and the third phenomena is the oxidation. The oxidation of the SiMo SGI and Fe-Si alloys is normally taking place in two steps [5,6]. Firstly, a thin and protective Si-rich oxide scale is produced, and secondly, nodules iron oxide nucleates formed at fast-growing level which producing a mixed scale formation with complex kinetics [7]. The presented nodules develop transversely until they cover up the whole surface of the sample. The resulting scale of Hi-SiMo SGI, is multi-layered with outward growing hematite, iron oxides, and magnetite beside an inward growing magnetite subscale, fayalite, and Si-rich oxide at the interface of the metal-oxide [8,9]. Though the main reason of initiation the iron oxide nodules on Fe-Si alloys is still not obvious, it is frequently attributed to combustion of graphite on SGI [7-9]. Increasing content of the Si helps formation of Si-rich oxide scale at the interface of the metal-oxide, such as fayalite (Fe_2SiO_4) and silica (SiO_2). The oxide layers represent the diffusion barriers and are capable for decreasing the thickness of the scale and oxidation kinetics even with the presence of the discontinuous [1,10,11]. The components of the exhaust are usually subjected to both combustion gas and ambient air. Combustion gas in the diesel engine is mainly carbon dioxide, nitrogen, and water vapor.

As diesel combustion takes place at high air/fuel ratio, combustion gas also presents large amounts of oxygen [12]. A studied SiMo SGI oxidation in diesel exhaust gases and established the key role of water vapor in the oxidation mechanism over carbon dioxide and nitrogen oxides [8,13]. A group researcher on Fe-1.5Si alloys in different H_2O containing atmospheres demonstrated that water vapor has accelerated the nucleation process of the iron oxide nodules, increased the oxidation kinetics, and finally led to porous iron oxide scales [14]. Parent-Simonin et al advised that vapor of water might have a critical impact on SGI decarburization as well [15]. Though, water vapor effect on oxidation mechanisms of Fe-Si alloys and SGI decarburization with high Si-content remains poorly understood. The properties and microstructures of the resulted cast iron alloys are largely depending on the alloying elements. Aluminum, as an example of the alloying elements, is one of the vital elements that supplemented to the cast iron in order to produce a new material with outstanding properties [16-32]. Addition of Al to the cast iron can produce other alloys with higher tensile strength, high thermal shock resistance, higher tendency for graphitizing, higher resistance for scaling at higher level of temperature, and good machinability [33-41]. Cast iron alloyed with Aluminum is used in several important applications, such as the main house of turbo-charge, exhaust manifolds, brake disc and drum, cylinder liners, rings of piston, camshafts, doors of coke oven and furnace trays used for heat treatments [42, 43].

The metal matrix microstructures and the graphite form in the cast iron are largely influenced by the content of the Al [44]. The formation of graphite promoted in the presence of Al in the cast iron. In addition, the presence of Al lead to stabilize the pearlite phase during the eutectoid transformation phase [45,46]. Next, Al shows similar effect of Si. Both of them dissolves in ferrite and austenite when their values are high. However, its solubility is low in carbides [46-48]. Some literatures showed that addition of Al to cast-iron increased the graphite nucleation tendency [49-51]. The similar effect of the graphitization of both Al and Si; Al replaces the silicon by increasing it values to be more than the silicon [52, 53]. However, both of them are added together with a considerable effect in order to get specific properties [49]. The Al-cast iron alloys are divided into two types. The first and the second contain up to 6% and 18 to 25% of the Aluminum, respectively [52-54]. For the alloys that contain up to 4%, all carbon precipitated as a graphite. Though, the aluminum effectiveness as a graphitizer decreased with increasing it ratio (6-12%). For the alloys of 8–18% of the aluminum, the appearance of the cast-iron is white as it contains complex iron aluminum carbides [55]. Aluminum start to recover it effectiveness of the graphitization and the

carbon starts to precipitate as a discrete graphite in a ferritic matrix as the aluminum ratio increase to 18%. The structural zones and their exact limits are affected by several factors, the Si content as a chemical composition, cooling rate, trace element, and treatment of graphite Spheroidising [44,55]. The Al-cast iron alloys and its properties are not totally exposed yet especially when it added with a ratio greater than 6% [43-46, 56-60]. Therefore, more studies are needed to understand its properties properly. This understanding will help the designers to use these alloys in several important applications, such as engines manifold that requires high capacity of damping at the higher values of oxidation rates [60,61].

In addition, the generated alloys of the Al and cast iron can be introduced as a very special candidate for a high temperature-oxidation atmosphere resistance, because of presenting of the scales of alumina, such as α -Al₂O₃, that shows outstanding temperature resistance. The aluminum scales work as barriers for diffusions during the process of oxidation at the high level of temperatures [62]. The industrial casting of boilers the produced from the cast iron that contained of aluminum with 5-7% and 0.7-1% showed 6-8 times of the longer time than the heat resistance of medium silicon of the ductile cast iron operating at 1000°C[63]. In their research, Kinai and Edmonds [64], showed that an adherent and very thin film of oxide of aluminum is produced in the presence of aluminum in the cast iron. This oxide works as a protector to the alloy from some attackers. The thickness of the oxide layers of the decreased as content of aluminum increased. This study concentrates on the aluminum addition effect in the cast iron on the resulted phase and oxidation resistance beside the relationship between them.

PREPARATION OF SAMPLES

Melting and Casting

To investigate the behavior of oxidation resistance of aluminum-bearing gray cast iron alloyed with different rates aluminum and obtaining the alloy compound with appropriate oxidation resistance, three samples of gray cast iron were casted with the 2, and 4 wt.% Al. Appropriate composition of raw cast iron slab and pure aluminum slab (99.8%) were used to prepare the melt for the considered cast irons. Low-carbon steel scrap was used to adjust and reduce the amount of carbon and silicon in the composition of cast irons. Silica lined coreless induction furnace was used for melting the material and appropriate control of the melting temperature. Since the melting temperature of aluminum is almost half the melting temperature of gray cast iron and a high percentage is oxidized by adding aluminum to the cast iron, the aluminum slabs were melted in a separate ladle, and the molten cast iron in another ladle was added to it. Then, the prepared molten material was gently stirred with a ceramic rod, poured at 1350 and 1400 °C range of the temperatures in a sand mold for production a test bar of 200 mm and 25 mm for the length and diameter, respectively.

Analysis of Chemical Composition

Chemical composition analysis of alloys (Base B, B1 and B2,) have been checked by X-Ray Fluorescent (XRF), using metal analysis by SPECTROMAX, (Germany) listed in Table 1.

Table 1. The chemical components and composition of aluminum cast-irons (wt%)

Sample No.	Chemical Composition							
	Al	C	Si	Cr	Mn	Ni	P	S
Base B	0	3.12	2.68	0.31	0.31	0.02	0.06	0.03
B1	2.3	3.78	1.93	0.45	0.29	0.07	0.02	0.07
B2	4.7	4.23	2.57	0.62	0.38	0.06	0.07	0.04

Heat Treatment

The process of homogeneous conducted at a temperature (750°C) in order to homogenize the composition, to ensure the distribution of the elements and inclusions on a regular basis in the alloy. Time residence is (6 hrs.) at this temperature, and leave them cooling slowly in the furnace, the alloys will be gained homogenous properties by this process.

Samples Preparation

The samples have been sectioned from test bars in order to prepare samples (Base B, B1, and B2) alloys into discs shaping with 20 mm and 4.5 mm in diameter and thick, respectively, were partitioned from test bars according to (ASTM G54-84, 1988) [65] Rough polishing was performed on the successively finer grades of emery papers. Different silicon carbide papers ranging from (80, 120, 180, 220, 400, 600, 800, 1000, 1200, 2000, 2500, and 3000) grid silicon carbide papers. Polishing was carried out by the polishing cloths via using diamond past. Polishing was done by diamond with particle size (1 μ m). Water was used as a coolant and lubricant to facilitate hand grinding. These samples were cleaned with distilled water and the alcohol. After drying in hot air, the samples are stored in polyethylene bags. The dimensions of all samples have been measured.

The Tests

Microstructure Test

The samples are imaged after grinding of up to (3000) grit and finally polishing by 0.25 μ m diamond, then they have been etched using the standard polish for cast irons (PN-61/H-0503) which consist of 4% of alcoholic nitric acid ("nital") at room temperature to disclose the boundaries of ferrite grain and disclose the produced phases and the corresponding constituents, such as pearlite and cementite [66]. After these processes, the samples are ready for microstructure test by using a light optical microscope (LOM). This test was involved identification and measurement of the phases & shape. The microstructure evaluated with (200X and 400X) magnification

X-Ray Diffraction (XRD)

Samples with (20mm) in diameter and (4.5 mm) in thickness have been prepared for X-Ray Diffraction analysis. The measure conditions are (Target: wavelength of 1.54060, Cu, 30 KV and 15 mA, for voltage and current, respectively, 2 deg./min for speed of scan, scanning range of ($2\theta = 0$ to 100 degrees). The X-Ray Diffraction was used in order to find the phases produced after heat treatment, and then compare it with the standard charts.

Cyclic Oxidation Tests

This test conducted in air at high temperature was achieved to study the resistance of oxidation of samples. The evaluations of the resistance of oxidation of the samples have been done by samples heating in a furnace at testing temperatures. The samples are weighed every 5 hrs. Then, the samples were removed from the furnace, left them to be cooled, cleaned by using ethanol for detaching the spall oxide. In addition, the change of weight rate per unit surface area was calculated. Samples were precisely weighed and then put into a ceramic crucible. The tests of the cyclic oxidation were carried out at a furnace with the temperatures range (700-900) °C in air at (1 atm.) pressure. Each heating cycles includes 5 hours of heating inside the furnace at the testing temperature and cooling outside the furnace. The changes in the samples' weight prior and after each cycle of oxidation were measured. Typically, at least 10 measurements of the weight were carried.

RESULTS AND DISCUSSION

Microstructure Examination

The microstructural analysis using optical microscopy of the cast-irons for various aluminum content indicated a formation of different phases. Figure 1 show some of the microstructural analyses. Various shapes with different distribution and sizes of the structural elements were noticed. The structural influences were subjugated by a noteworthy increasing in ferrite percent at the high content of Al. The various presented phases were mainly pearlite, α -iron, and graphite. It was noticed that the ferrite represents the main matrix component when the aluminum added to the cast iron within 2.3 and 4.7 % while the graphite presented in a shape of flakes. The morphology of the graphite and its distribution was not the same compared to the cast iron without aluminum addition. In addition, as aluminum percentage increase, the volume fraction of the pearlite increases as well.

Cyclic Oxidation Test

The test of cyclic oxidation was performed for all alloys (B, B1, and B2), at high temperature and at environment of air. The protective oxide layer resistance evaluation was achieved by heating the samples inside the furnace with temperature equal to testing temperature and weighting them each five hours. Samples were taken outside the furnace and left them to cool in still air. Then they were cleaned by detaching the spalled oxidation. The

change in the weight divided by the unit surface area was determined in accordance with the procedure [67]. Figure 2 represents oxidation behavior of reference sample B, for different temperatures (700, 800, 900) °C. Its behavior is expected (stratified), due to nature of oxide film which build on alloy surface, this layer is porous, thick, and non-adhesive.

The first oxidation process typically begins with the graphite flakes oxidation that were exposed to environmental air and subsequently with the oxidation of the exposed alloying elements. During this time, if the variation in the weight was pointed to the negative weight loss, it was then attributed to the high carbon oxidation rate when in comparison with the metal oxidation. The next oxidation process normally showed a gain in the weight by forming scales of iron oxide that overcame the loss of weight by decarburization. The observed oxidation kinetics of alloy B (without aluminum) was attributed to the accumulation (i.e. gain in the weight) of iron oxide combined influences, while the loss in the weight was attributed to decarburization. If the graphite consumption at the surface surpasses the relative gain in weight owing to iron oxidation, the change in the weight will appear negative. Whereas, exceeding the gain in the weight by oxide formation over the decarburization loss led to increasing the total change in the weight. Cavities (gaps) were left after consumption of the graphite, and thereby these iron oxides had the ability of filling these holes and thus providing anchors which could key the metal's scale. Cracking the scale and spalling or partially spalling results in the variation in the rate of weight change.

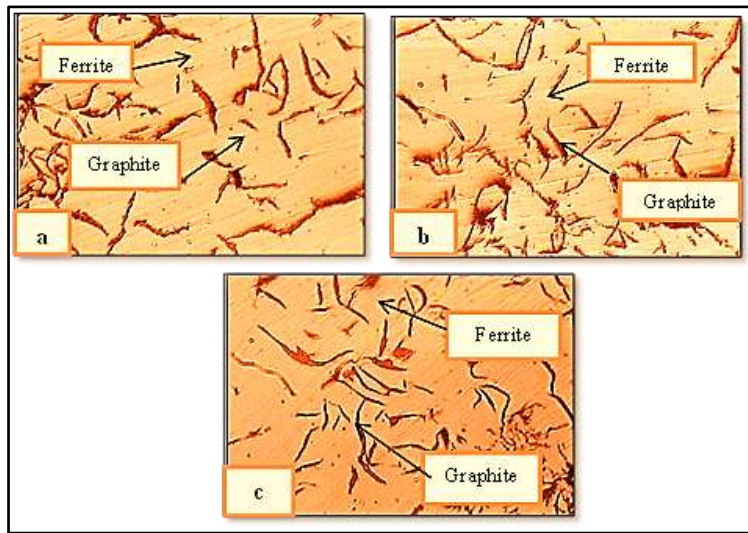


Figure 1. The alloyed cast-irons microstructure with various contents of Al: (a) Alloy B, (b) alloy B1, and (c) alloy B2

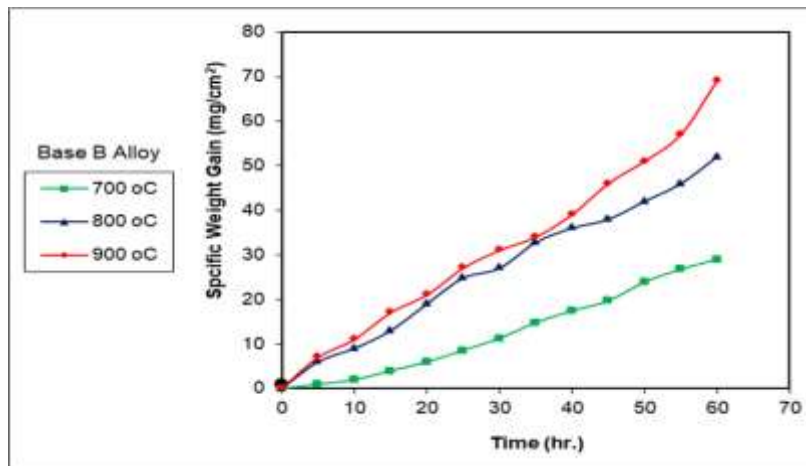


Figure 2. Specific weight gain of alloy B (gray cast iron) oxidized in atmospheric air with temperatures between 700- 900°C

The cracks presence in the oxide layer resulted in a significant increasing in the surface area that exposed to the oxygen, which contributed to accelerate the oxidation kinetics (Figure 3). After the period of oxidation at 700, 800 and 900 °C (first stage), it was observed that the formation of the scale on the alloy B had a propensity of spalling from the surface during cooling process. Once the scale was spalled away from the surface, a new scale has been formed on the surface due to oxidation process, but with stronger adhesion with the subsurface. At high temperatures, the formed scale on oxidized cast iron was consisted of various layers with various types of iron oxides such as Fe_3O_4 , Fe_2O_3 and FeO .

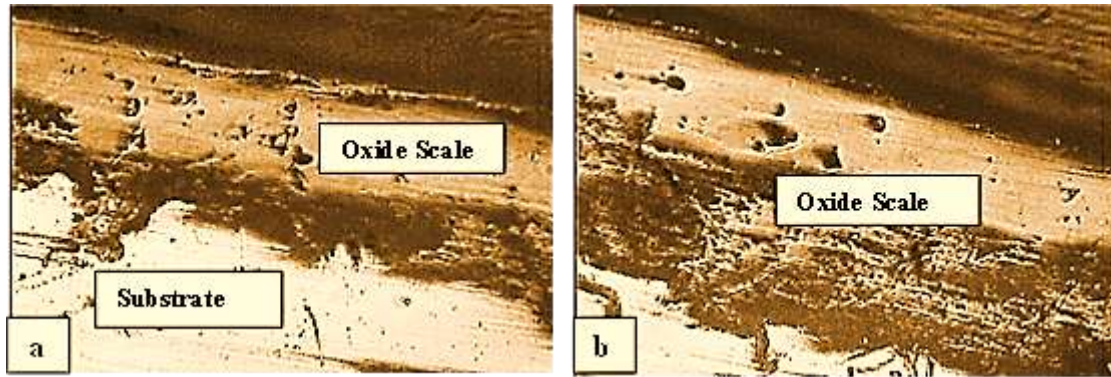


Figure 3. Cross sectional images of alloy B (gray cast-iron) that oxidized in atmospheric air for 60 hrs at 5 hr cycle: (a) 700°C, and (b) 900°C

The specific weight gain data of the alloy B1 for each temperature test is plotted in Figure 4 versus the time. The initial kinetic was fast, but the rate of the specific weight change was gradually reduced with time increasing. Kinetics can be described by checking the value of the rate time constant (index n) in the rate equation below [68]:

$$\Delta W/A = k t^n \quad (1)$$

Symbol ΔW denotes the weight change, A denotes the surface area of the sample, k denotes the rate constant, n denotes the constant of growth-rate time, and t denotes the oxidation time. When the temperature is 700°C, the best fitting gives an index n that approximately equal to 0.59 (i.e., parabolic behavior). Other values of the index n are listed in Table 2. The results showed that when the value of the index n is equal to 0.5, the relationship is parabolic. The index n can describe the rate of oxidation as follows: when n equals to 1, 0.5, and 0.33, the rate of oxidation is linear, parabolic, and cubic respectively [68].

If the index n is less or more than 0.5, the oxidation kinetic won't behave simple parabolic relation and this indicates a slower or faster rate of oxidation. Under parabolic or so-called sub-parabolic rate was taken place when $n < 0.5$; while, over-parabolic rate was occurred when $n > 0.5$. The findings revealed that sub-parabolic might be found due to mechanisms of the grain boundaries (short circuits). Shifting of index n from the theoretical (i.e. 0.5) could be interpreted by a cracking of an oxide layer, resulting in a rapid increase of the surface area that exposed to oxygen and thereby increasing the kinetics of oxidation. In addition, experimental conditions and several variables such as measurement of weight and area, and others, can play a key role in this situation [69].

At the temperature range used in this work, the oxidation kinetic could be computed using a modified law of parabolic rate by assuming the diffusion mechanism controlling the oxidation and the only efficient short-circuit diffusion paths were the grain boundaries. High rate of oxidation was initially provided by the diffusion mechanism of grain boundaries. Growing of the oxide grain increased with time and this led to decrease the easy diffusion path numbers; therefore, the rate of oxidation became slow. Consequently, the easy pathways almost vanished, and the rate of oxidation decreased beyond that for parabolic kinetics [70].

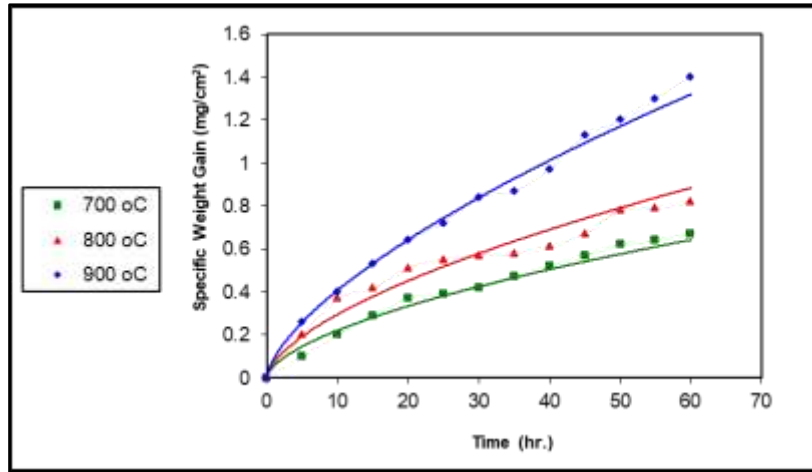


Figure 4. The relationship between the specific weight gain and time with parabolic fitted of alloy B1 cyclic oxidized in atmospheric air at temperatures ranged from 700 to 900 °C for 60 hrs at 5 hrs cycle.

The rate equation for the parabolic kinetics is [70]:

$$\Delta W/A = k t^{0.5} \quad (2)$$

The symbol k now denotes to parabolic rate constant. The slope of any straight line of the relationship between the specific weight gain and square root of time in Figure 5 represents the constant of parabolic rate in units of $(\text{mg}/\text{cm}^2)/\text{hr.}^{1/2}$. The value of k in equation (2) was squared to get k_p in units of $(\text{mg}^2/\text{cm}^4)/\text{hr.}$, as per Equation (3):

$$(\Delta W/A)^2 = k_p t \quad (3)$$

Using the same procedure, the specific weight gain values of the B2 alloy at different times for the specified temperatures are shown in Figure 6.

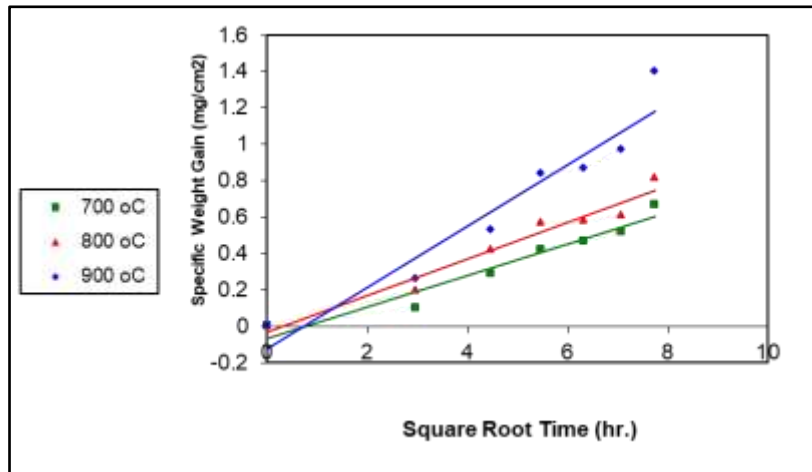


Figure 5. Linear fitting of the specific weight gain data vs. $t^{0.5}$ for B1 alloy cyclic oxidized in atmospheric air with temperatures equal to 700, 800 and 900 °C for 60 hrs at 5 hrs cycle.

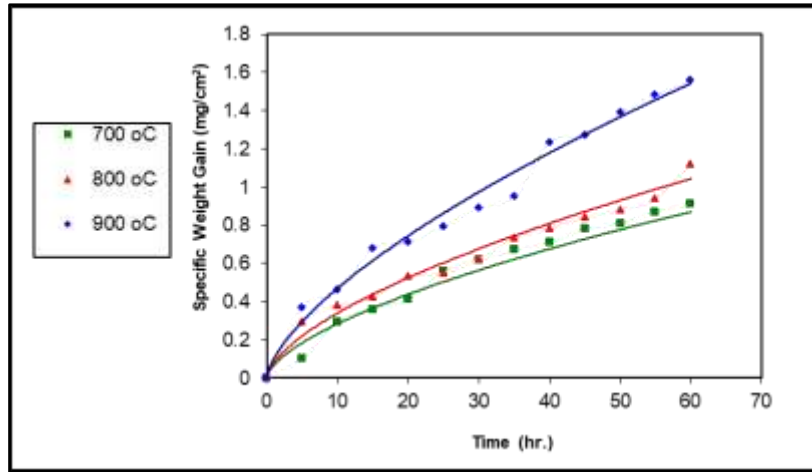


Figure 6. Parabolic fitting of the specific weight gain data vs. time for alloy B2 cyclic oxidized in atmospheric air with temperatures equal to 700, 800 and 900 °C for 60 hrs at 5 hrs cycle.

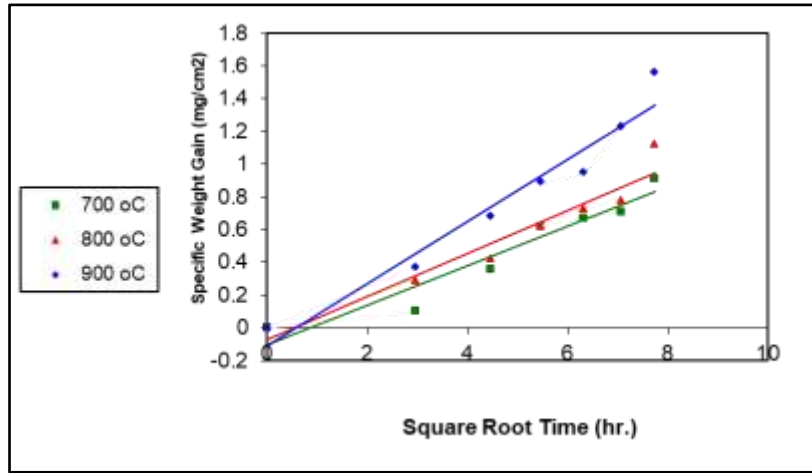


Figure 7. Linear fitting of the specific weight gain data vs. $t^{0.5}$ for B2 alloy cyclic oxidized in atmospheric air with temperatures equal to 700, 800 and 900 °C for 60 hrs at 5 hrs cycle.

The k_p for B1 and B2 alloys of experiments were computed and the straight lines represented the least squares fitting of the data in Figures 5, and 7. Table 2 lists the constants k_p for set of experimental tests.

Table 2. n and k_p values for cyclic oxidation of alloy B1 and B2 in atmospheric air for 60 hrs at 5 hrs cycle.

	Temperature (°C)	n values	k_p (mg^2/cm^4)/s.
Alloy B1	700	0.59	8.773×10^{-7}
	800	0.61	14.561×10^{-7}
	900	0.65	22.853×10^{-7}
Alloy B2	700	0.62	12.462×10^{-7}
	800	0.63	17.912×10^{-7}
	900	0.66	28.783×10^{-7}

The k_p values and thus the rate of oxidations of B1 alloys in air increased from 8.773×10^{-7} to 22.853×10^{-7} (mg^2/cm^4)/s at temperatures 700 and 900 °C, respectively. Meanwhile, k_p values for B2 alloys increased from 12.462×10^{-7} to 28.783×10^{-7} (mg^2/cm^4)/s at temperatures 700 and 900 °C, respectively. It is worth mentioning that the gain in weight (ΔW) obtained by substituting k_p listed in Table 2 in Equation 3 resulted in the oxygen gained weight by the sample under cyclic oxidation. Table 2 shows that lower content of the aluminum led to less change in the kinetic oxidation. The oxide-ability in the cast-irons having low aluminum content increased with increasing the temperature. Differential contraction of the metal and oxide scales during thermal cycle could be responsible

for the formation of voids and cracks. The formation of oxide along the graphite flakes and gases penetration into cast iron led to volume increasing due to the formation of voids and cracks.

The formed oxide layers on the surface of B and B2 alloys (0 and 4.7% Al) are shown in Figures 3 and 8. These layers were anticipated to obstruct the oxidation. Cast iron oxidation containing low aluminum was controlled by the outward transfer of iron ions in the scale. Therefore, the oxidation rates reduced as Al content increased. Aluminum's solubility in iron oxides caused changes in the oxide properties and thereby changing the retardation of diffused iron ions. External protective scales were initially formed, as in any alloyed cast iron; these scales undergo cracking and spalling in a short time. Consequently, a second or a third scale that influences the oxidation rate was noted (Fig. 8). The sample released small particles, and this provided an evidence that the alloy had an oxidized behavior.

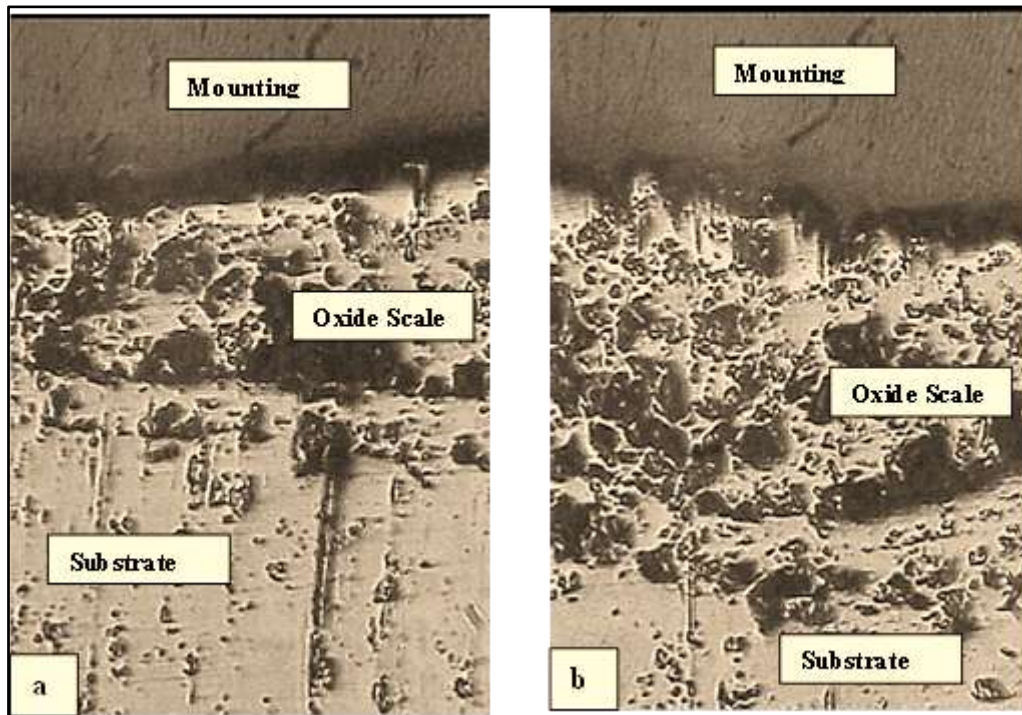


Figure 8. Cross sectional images of alloy B2 (cast iron) oxidized in atmospheric air for 5 hrs at: (a) 700°C and (b) 900 °C

CONCLUSIONS

1. Addition of aluminum to the molten (cast-iron) with attention being taken into consideration compensating the value of the lost aluminum by about 15% due to the difference between the melting temperature of the two materials as the aluminum is largely lost due to oxidation at high temperatures and burning large amounts of it.
2. The resulting slag increases significantly after adding aluminum to the molten, which in turn plays the role of slag insulation due to the high affinity of oxygen.
3. Aluminum acted as a strong graphitizing material and at the same time enriched with the formation of graphite slices, which was similar to the role of silicon in addition to the phases consisting of graphite and ferritic matrix.
4. The specific weight gain increased with an increase in oxidation temperature when stabilizing the proportion of aluminum (at the ratio of one aluminum). Thus, the resistance to oxidation decreased by forming a non-protective flak layer that was not adherent to the surface, as oxygen absorption increases, and the alloy fails. Thus, the sample weight increased, and with the increase in the amount of graphite, the peeling ratio increased, and its highest value reached a temperature of 900°C.

5. The specific weight gain decreased with an increase in the percentage of aluminum in alloy cast iron with stabilization of the temperature (at one temperature) due to the formation of a surface layer adhering to the surface and its best value was obtained at a temperature of 900°C and the percentage of aluminum is 4.7%.
6. Aluminum played an important role in changing the condition of the microstructure. The composition of the matrix included different ratios of perlite, ferrite, and graphite.
7. There was no sign of spalling at temperatures ranged from 700 to 900 °C in aluminum-alloyed cast-irons. The rate of oxidation in the aluminum-alloyed cast-iron decreased with increasing the content of aluminum.

REFERENCES

- [1] A.A. Partoaa, M. Abdolzadeh, and M. Rezaeizadeh, “Effect of fin attachment on thermal stress reduction of exhaust manifold of an off road diesel engine”, *J. Cent. South Univ.*, Vol. 24, No. 3, Pp. 546, 2017.
- [2] Y.H. Zhang, M. Li, L.A. Godlewski, J.W. Zindel, and Q. Feng, “Creep behavior at 1273 K (1000°C) in Nb-bearing austenitic heat-resistant cast steels developed for exhaust component applications”, *Metall. Mater. Trans. A*, Vol. 47, No. 7, Pp. 3289, 2016.
- [3] M. Ekström, and S. Jonsson, “High-temperature mechanical and fatigue properties of cast alloys intended for use in exhaust manifolds”, *Mater. Sci. Eng. A.*, Vol. 616, Pp. 78, 2014.
- [4] L.M. Åberg and C. Hartung, “Solidification of SiMo nodular cast iron for high temperature applications”, *Trans. Indian Inst. Met.*, Vol. 65, No. 6, Pp. 633.
- [5] J.P. Shingledecker, P.J. Maziasz, N.D. Evans, and M.J. Pollard, “Creep behavior of a new cast austenitic alloy”, *Int. J. Press. Vessels Pip.*, Vol. 84, No. 1-2, Pp. 21, 2007.
- [6] M.M. Ibrahim, A. Nofal, and M.M. Mourad, “Microstructure and hot oxidation resistance of SiMo ductile cast irons containing Si–Mo–Al”, *Metall. Mater. Trans. B.*, Vol. 48, No. 2, Pp. 1149, 2017.
- [7] Y.H. Zhang, M. Li, L.A. Godlewski, J.W. Zindel, and Q. Feng, “Effective design of new austenitic cast steels for ultra-high temperature automotive exhaust components through combined CALPHAD and experimental approaches”, *Mater. Sci. Eng. A.*, Vol. 683, Pp. 195, 2017.
- [8] F. Tholence and M. Norell, “High temperature corrosion of cast alloys in exhaust environments I-ductile cast irons”, *Oxid. Met.*, Vol. 69, No. 1-2, Pp. 13, 2008.
- [9] M. Ekström, P. Szakalos, and S. Jonsson, “Influence of Cr and Ni on high-temperature corrosion behavior of ferritic ductile cast iron in air and exhaust gases”, *Oxid. Met.*, Vol. 80, No. 5-6, Pp. 455, 2013.
- [10] F. Tholence and M. Norell, “High temperature corrosion of cast alloys in exhaust environments II-cast stainless steels”, *Oxid. Met.*, Vol. 69, No. 1-2, Pp. 37, 2008.
- [11] Y.H. Zhang, M.L. Larry, L.A. Godlewski, J.W. Zindel, and Q. Feng, “Effects of W on creep behaviors of novel Nb-bearing high nitrogen austenitic heat-resistant cast steels at 1000°C”, *Mater. Charact.*, Vol. 139, Pp. 19, 2018.
- [12] M.P. Brady, G. Muralidharan, D.N. Leonard, J.A. Haynes, R.G. Weldon, and R.D. England, “Long-term oxidation of candidate cast iron and stainless steel exhaust system alloys from 650 to 800°C in air with water vapor”, *Oxid. Met.*, Vol. 82, No. 5-6, Pp. 359, 2014.
- [13] G.M.C. Güiza, W. Hormaza, A.R. Galvis E, and L.M.M. Morenod, “Bending overload and thermal fatigue fractures in a cast exhaust manifold”, *Eng. Fail. Anal.*, Vol. 82, Pp. 138, 2017.
- [14] J.W. Soedarsono, T.P. Soemardi, B. Suharno, and R.D. Sulamet Ariobimo, “Effects of carbon equivalent on the microstructures of thin wall ductile iron”, *J. Mater. Sci. Eng.*, Vol. 5, No. 3, Pp. 266, 2011.
- [15] G.E. Totten, “Steel Heat Treatment Handbook”, Chemical Rubber Company Press, Boca Raton, 2006.
- [16] H. Bhadeshia and R. Honeycombe, “Steels: Microstructure and Properties”, Elsevier, Oxford, 2006.

- [17] A.R.K. Rashid and D.V. Edmonds, "Oxidation behaviour of Al-alloyed ductile cast irons at elevated temperature", *Surf. Interface Anal.*, Vol. 36, No. 8, Pp. 1011, 2004.
- [18] A. Hassani, A. Habibolahzadeh, and S. Sadeghinejad, "Comparison of microstructural and tribological effects of low vanadium–low titanium additions to a gray cast iron", *J. Mater. Eng. Perform.*, Vol. 22, No. 1, Pp. 267, 2013.
- [19] T.N.F. Souza, R.A.P.S. Nogueira, F.J.S. Franco, M.T.P. Aguilar, and P.R. Cetlin, "Mechanical and microstructural characterization of nodular cast iron (NCI) with niobium additions", *Mater. Res.*, Vol. 17, No. 5, Pp. 1167, 2014.
- [20] Y.Z. Lv, Y.F. Sun, J.Y. Zhao, G.W. Yu, J.J. Shen, and S.M. Hu, "Effect of tungsten on microstructure and properties of high chromium cast iron", *Mater. Des.*, Vol. 39, Pp. 303, 2012.
- [21] C. Delprete and R. Sesana, "Experimental characterization of Si–Mo–Cr ductile cast iron", *Mater. Des.*, Vol. 57, Pp. 528, 2014.
- [22] A. Bedolla-Jacuinde, E. Solis, and B. Hernandez, "Effect of niobium in medium alloyed ductile cast irons", *Int. J. CastMet. Res.*, Vol. 16, No. 5, Pp. 481, 2003.
- [23] D.X. Zeng, Y.H. Zhang, J.Y. Liu, H.J. He, and X.X. Hong, "Characterization of titanium-containing compounds in gray iron", *Tsinghua Sci. Technol.*, Vol. 13, No. 2, Pp. 127, 2008.
- [24] M. Gómy and M. Kawalec, "Effects of titanium addition on microstructure and mechanical properties of thin-walled compacted graphite iron castings", *J. Mater. Eng. Perform.*, Vol. 22, No. 5, Pp. 1519, 2013.
- [25] X.R. Chen, J. Xu, H. Hu, H. Mohrbacher, M. Kang, W. Zhang, A.M. Guo, and Q.J. Zhai, "Effects of niobium addition on microstructure and tensile behavior of as-cast ductile iron", *Mater. Sci. Eng. A.*, Vol. 688, Pp. 416, 2017.
- [26] T. Elbel and J. Hampl, "Influence of Al and Ti on microstructure and quality of compacted graphite iron casting", *Metalurgija*, Vol. 48, No. 4, Pp. 243, 2009.
- [27] M. Gómy and M. Kawalec, "Role of titanium in thin wall vermicular graphite iron casting production", *Arch. Foundry. Eng.*, Vol. 13, No. 2, Pp. 25, 2013.
- [28] C.A. Cooper, R. Elliott, and R.J. Young, "Investigation of elastic property relationships for flake and spheroidal cast irons using Raman spectroscopy", *Acta Mater.*, Vol. 50, No. 16, Pp. 4037, 2002.
- [29] H. Nakae and H. Shin, "Effect of graphite morphology on tensile properties of flake graphite cast iron", *Mater. Trans.*, Vol. 42, No. 7, Pp. 1428, 2001.
- [30] D. Holmgren, A. Diószegi, and I.L. Svensson, "Effects of nodularity on thermal conductivity of cast iron", *Int. J. Cast Met. Res.*, Vol. 20, No. 1, Pp. 30, 2007.
- [31] P. Bastid, P. Pilvin, C. Grente, and E. Andrieu, "Microstructural Evolution of Spheroidal Graphite Cast Iron at High Temperature: Consequences on Mechanical Behaviour", *Adv. Mat. Res.*, Vol. 4–5, Pp. 139–146, 1997.
- [32] Y. Yamaguchi, S. Kiguchi, H. Sumimoto, and D.K. Nakamura, "Effect of graphite morphology on decarburized cast iron", *Int. J. Cast. Metal Res.*, 16, Pp. 137–142, 2003.
- [33] L.L. Liu, Q.Q. Guo, and Y. Niu, "Transition Between Different Oxidation Modes of Binary Fe–Si Alloys at 600–800 °C in Pure O₂", *Oxid Met.*, Vol. 79, Pp. 201–224, 2013.
- [34] M. Ekström, P. Szakalos, and S. Jonsson, "Influence of Cr and Ni on High-Temperature Corrosion Behavior of Ferritic Ductile Cast Iron in Air and Exhaust Gases", *Oxid Met.*, Vol. 80, Pp. 455–466, 2013.
- [35] F. Tholence, and M. Norell, "High-Temperature Corrosion of Cast Irons and Cast Steels in Dry Air", *Materials Science Forum*, Vol. 369–372, Pp. 197–204, 2001.
- [36] I. Svedung, and N.G. Vannerberg, "The influence of silicon on the oxidation properties of iron", *Corros. Sci.*, Vol. 14, Pp. 391–399, 1974.

- [37] A. Atkinson, "A theoretical analysis of the oxidation of Fe–Si alloys", *Corros. Sci.*, Vol. 22, Pp. 87–102, 1982.
- [38] J.B. Heywood, "Internal combustion engine fundamentals", McGraw-hill New York, 1988.
- [39] F. Tholence, and M. Norell, "High Temperature Corrosion of Cast Alloys in Exhaust Environments -Ductile Cast Irons", *Oxid Met.*, Vol. 69, Pp.13–36, 2008.
- [40] M. Fukumoto, S. Maeda, S. Hayashi, and T. Narita, "Effect of Water Vapor on the Oxidation Behavior of Fe–1.5Si in Air at 1073 and 1273 K", *Oxid Met.*, Vol. 55, Pp. 401–422, 2001.
- [41] S. Parent-Simonin, C. Moreaux, and J.C. Margerie, "Influence of the Annealing Atmosphere on the Structure of Malleable Cast Irons", *Rev. Metall.*, Vol. 74, Pp. 537–543, 1977.
- [42] J.R. Davis, "Cast iron. In: JR Davis, editor. ASM specialty handbook", 1st ed., Metals Park (OH); ASM International, Pp. 32–154, 1996.
- [43] A.R. Kiani-Rashid, and D.V. Edmonds, "Phase transformation study of aluminium-containing ductile cast irons by dilatometry", *Mater. Sci. Eng. A.*, Vol. 481, Pp. 752–756, 2008.
- [44] M.S. Soinski, A. Jakubus, and P. Kordas, 2014. "The effect of aluminium on graphitization of cast iron treated with cerium mixture", *Arch. Foundry Eng.*, Vol. 14, Pp. 95–100.
- [45] D.M. Stefanescu, and F. Martinez, "Compacted/vermicular graphite cast irons in the Fe-C-Al System", *AFS Trans.*, Vol. 39, Pp. 39–46, 1982.
- [46] A. Shayesteh-Zeraati, H. Naser-Zoshki, and A.R. Kiani-Rashid, "Microstructural and mechanical properties (hardness) investigations of Al-alloyed ductile cast iron", *J. Alloys Compd.*, Vol. 500, Pp. 129–133, 2010.
- [47] S.K. Yu, and C.R. Loper, "Effect of molybdenum, copper and nickel on the pearlitic and martensitic hardenability of ductile iron", *AFS Trans.*, Vol. 96, Pp. 811–822, 1988.
- [48] D.M. Stefanescu, "Thermodynamic properties of iron-base alloys", *ASM Handbook, metals handbook*, 9th ed. Metals Park (OH): ASM International, Vol. 15, Pp. 61–70, 1992.
- [49] R.J. Smickley, and K.B. Rundman, "The effect of aluminum on the structure and properties of grey cast iron", *AFS Trans.*, Vol. 89, Pp. 205–214, 1981.
- [50] A.R. Kiani-Rashid, and D.V. Edmonds, "Graphite phase formation in Al-alloy ductile iron", *IJE Trans. B.*, Vol. 15, Pp. 261–272, 2002.
- [51] A.R. Kiani-Rashid, and M.A.Golozar, "Microscopic segregation pattern of Al and Si in matrix microstructure of cast irons with spherical graphite", *Esteghlal J.*, Vol. 2, Pp. 177–188, 2003.
- [52] N. Haghdam, B. Bazaz, and H.R. Erfanian-Naziftoosi, "Microstructural and mechanical characteristics of Al alloyed ductile iron upon casting and annealing", *Int. J. Miner. Meta. Mater.*, Vol. 19, Pp. 812–820, 2012.
- [53] H.R. Erfanian-Naziftoosi, N. Haghdam, and A.R. Kiani-Rashid, "The effect of isothermal heat treatment time on the microstructure and properties of 2.11% Al austempered ductile iron", *J. Mater. Eng. Perform.*, Vol. 21, Pp. 1785–1792, 2012.
- [54] C.F. Walton, and T.J. Opar, "Iron castings handbook", New York: Iron Castings Society, Pp. 427–439, 1981.
- [55] A.A. Nofal, N.S. Felix, and A.S. Rizk, "Cast iron alloyed with 9% Al", 50th International Foundry Congress, Nov 6–11; Paper No.10; Cairo, Egypt, 1983.
- [56] S.K. Shaha, M.M. Haque, and A.A. Khan, "Study on the microstructure and properties of Fe-C-Si and Fe-C-Al cast irons", *Adv. Mater. Res.*, Vol. 264, Pp. 1933–1938, 2011.
- [57] X. Liu, S. Takamori, and Y. Osawa, "Low-temperature damping behavior of cast iron with aluminum addition", *J. Mater. Sci.*, Vol. 40, Pp. 1773–1775, 2005.

- [58] T. Susumu, K. Takashi, and O. Yoshiaki, "Structure and wear properties of aluminum alloyed gray cast iron", *J. Found. Eng. Soci.*, Vol. 74, Pp. 3–8, 2002.
- [59] R. Elliott, "Cast iron technology", 1st ed., London: Butterworth.
- [60] L. Xinbao, S. Takamori, and Y. Osawa, "The effect of aluminum addition on the damping capacity of cast iron", *J. Mater. Sci.*, Vol. 39, Pp. 6097–6099, 2004.
- [61] S. Takamori, Y. Osawa, and K. Halada, "Aluminum-alloyed cast iron as a versatile alloy", *Mater. Trans.*, Vol. 43, Pp. 311–314, 2002.
- [62] S. Chevalier, C. Houngrinou., S. Paris, F. Bernard, E. Gaffet, Z.A. Munir, J.P. Larpin, and G. Borchardt, "Oxidation study of alumina-forming alloys", *The Journal of Corrosion Science and Engineering*, Vol. 6, Pp. H070, [online] Available <http://www.jcse.org.viewpreprint.php?vol=6, 2003 &pap=104>.
- [63] B.M.Z. Sun, and Z.F. Wang, "Development and application of Cr-Al heat-resistant alloys cast irons", *Foundry (China)*, Vol. 7, Pp. 31-34, 1996.
- [64] A.R.K. Rashid, and D.V. Edmonds, "Oxidation behaviour of Al-alloyed ductile cast irons at elevated temperature", *Surface and Interface Analysis*, Vol. 36, Pp. 1011-1013, 2003.
- [65] J.R. Nicholls, and M.J. Bennett, "Cyclic oxidation-guideline for test standardization, aimed at the assessment of service behavior", *Materials at High Temperatures*, Vol. 17, Pp. 413-428, 2000.
- [66] M.J. Kadhim, "Microstructure and High Temperature Oxidation Behavior of Aluminum Alloyed Cast Irons", *Modern Applied Science*, Vol. 4, Pp. 130-135, 2010.
- [67] P.C. Martinengo, C. Carughi, U. Ducati, and G.L. Coccia, "High Temperature Behavior of Protective Coatings on Ni – Base Superalloys", in: *Materials and Coatings to Resist High Temperature Corrosion*, Applied Science Pub. LTD, London, pp. 293-312, 1978.
- [68] D.F. Susan and A.R. Marder, "Oxidation of Ni-Al-Base Electrodeposited Composite Coatings. I: Oxidation Kinetics and Morphology at 800 oC", *Oxidation of Metals*, Vol. 57, Nos. 1/2, Pp. 131-157, 2002.
- [69] A.H. Hallem, and N.M. Dawood, "Investigation the effects of zirconium addition on wear and corrosion behaviour of alpha-brass alloy (Cu-Zn30)", *International Journal of Mechanical Engineering and Technology (IJMET)*, Vol. 9, No. 12, Pp. 844–857, 2018.
- [70] H. Kyung, and C.K. Kim, "Microstructural Evolution of Duplex Grain Structure and Interpretation of the Mechanism for NiO Scales Grown on Pure Ni – and Cr – Doped Substrate During High Temperature Oxidation", *Materials Science and Engineering*, B76, Pp. 173-183, 2000.